PNAS RESEARCH ARTICLE | BIOCHEMISTRY

The adaptive antioxidant response during fasting-induced muscle atrophy is oppositely regulated by ZEB1 and ZEB2

Chiara Ninfali[a], Marlies Cortés[a], M. C. Martínez-Campanario[a], Verónica Domínguez[b], Lu Han[a], Ester Tobías[c], Anna Esteve-Codina[d], Carlos Enrich[e], Belén Pintado[b], Gloria Garrabou[c], and Antonio Postigo[a,f,g,1]

Edited by Douglas Wallace, University of Pennsylvania, Philadelphia, PA; received January 20, 2023; accepted September 26, 2023

Reactive oxygen species (ROS) serve important homeostatic functions but must be constantly neutralized by an adaptive antioxidant response to prevent supraphysiological levels of ROS from causing oxidative damage to cellular components. Here, we report that the cellular plasticity transcription factors ZEB1 and ZEB2 modulate in opposing directions the adaptive antioxidant response to fasting in skeletal muscle. Using transgenic mice in which *Zeb1* or *Zeb2* were specifically deleted in skeletal myofibers, we show that in fasted mice, the deletion of *Zeb1*, but not *Zeb2*, increased ROS production and that the adaptive antioxidant response to fasting essentially requires ZEB1 and is inhibited by ZEB2. ZEB1 expression increased in fasted muscles and protected them from atrophy; conversely, ZEB2 expression in muscles decreased during fasting and exacerbated muscle atrophy. In fasted muscles, ZEB1 reduces mitochondrial damage and increases mitochondrial respiratory activity; meanwhile, ZEB2 did the opposite. Treatment of fasting mice with *Zeb1*-deficient myofibers with the antioxidant triterpenoid 1[2-cyano-3,12-dioxool-eana-1,9(11)-dien-28-oyl] trifluoro-ethylamide (CDDO-TFEA) completely reversed their altered phenotype to that observed in fasted control mice. These results set ZEB factors as potential therapeutic targets to modulate the adaptive antioxidant response in physiopathological conditions and diseases caused by redox imbalance.

antioxidant response | NRF2 | muscle atrophy | reactive oxygen species | ZEB1 and ZEB2

Significance

Reactive oxygen species (ROS) are normally produced by cells, but they must be constantly neutralized to prevent their supraphysiological levels from causing oxidative damage to cellular components. The study found that the transcription factors ZEB1 and ZEB2 activated and repressed, respectively, the adaptive antioxidant response to fasting in skeletal muscle. These findings suggest that ZEB factors could serve as potential therapeutic targets to modulate the antioxidant response in pathophysiological conditions.

Cells generate reactive oxygen species (ROS) as a byproduct of aerobic respiration. ROS play important homeostatic roles (e.g., proliferation, differentiation, migration, angiogenesis) and are also constantly neutralized by an adaptive antioxidant response of enzymes and small molecules (1). Alteration of this balance in the direction of supraphysiological levels of ROS leads to oxidative stress, characterized by the unspecific oxidation of biomolecules and alteration of normal cellular functions. Thus, oxidative stress has been linked, inter alia, to neurodegenerative disorders, cardiovascular diseases, diabetes, and cancer as well as to physiopathological and clinical conditions associated with muscle atrophy (1–4). Muscle atrophy occurs when protein degradation surpasses protein synthesis in a process involving the activation of two key protein degradation pathways: the ubiquitin–proteasome system and the autophagy–lysosome system (3, 5). In skeletal muscle, ROS are continually produced in response to myofiber contraction, and oxidative stress can both contribute to and be a consequence of muscle atrophy. On the one hand, oxidative stress triggers muscle atrophy through the upregulation of the two aforementioned protein degradation pathways; on the other hand, muscle atrophy increases ROS production (3, 5, 6).

The transcription factor NRF2 (encoded by *NFE2L2*) orchestrates an antioxidant response both in homeostasis and disease (reviewed in refs. 7 and 8). Under basal nonoxidative stress conditions, NRF2 cytoplasmic levels are maintained low through binding to KEAP1, an E3 ubiquitin ligase that targets NRF2 for degradation (9). The binding of ROS to reactive cysteine residues in KEAP1 induces a conformational change that inhibits the ubiquitination of NRF2, without affecting its binding to NRF2. This enables the accumulation of newly synthesized NRF2, facilitating its translocation to the nucleus where it transcriptionally activates genes involved in multiple pathways, including redox balance, proteostasis, metabolism, and autophagy (8, 10).

In the context of cancer, oxidative stress induces DNA mutagenesis and cell transformation, but malignant cells also exhibit enhanced NRF2-mediated antioxidant activity that allows them to overcome ROS-induced cell arrest and apoptosis thus favoring tumor growth (11, 12). In most scenarios, ROS activates an epithelial-to-mesenchymal transition (EMT) in cancer cells (12, 13), a cell dedifferentiation and plasticity reprogramming that promotes tumor progression. However, the interplay between oxidative stress and EMT is cell-specific and context-dependent, and ROS can also inhibit EMT in certain types of cancer cells. The EMT is orchestrated by a small set of transcription factors, including the

Author contributions: C.N. and A.P. designed research; C.N., M.C., and M.C.M.-C. performed research; C.N. and A.P. interpreted results; V.D., E.T., B.P., and G.G. contributed new reagents/analytic tools; C.N., L.H., A.E.-C., C.E., and A.P. analyzed data; A.P. conceived and supervised the project, obtained funding; and A.P. wrote the paper.

The authors declare no competing interest.

This article is a PNAS Direct Submission.

[1]To whom correspondence may be addressed. Email: idib412@recerca.clinic.cat.

This article contains supporting information online at https://www.pnas.org/lookup/suppl/doi:10.1073/pnas.2301120120/-/DCSupplemental.

Published November 10, 2023.

two members of the ZEB family, ZEB1 and ZEB2 (14–17). The above evidence prompted us to study the potential role of ZEB1 and ZEB2 in the regulation of ROS and the adaptive antioxidant response in the context of muscle atrophy.

Using transgenic mice where *Zeb1* or *Zeb2* have been specifically deleted in skeletal myofibers, we found that the adaptive NRF2-dependent antioxidant response during fasting requires ZEB1 and is inhibited by ZEB2. Altogether, the results presented here establish ZEB factors as potential therapeutic targets for diseases triggered by oxidative stress.

Results

***Zeb1* Deletion in Skeletal Myofibers, but Not *Zeb2*, Increases ROS Production in Response to Fasting.** We first examined whether fasting modulates ZEB1 and ZEB2 expression in skeletal muscle. Two-to-three-month-old wild-type mice were either allowed to eat ad libitum (hereinafter referred to as "fed" condition) or subjected to fasting for 36 h (referred to as "fasted"). Interestingly, fasting resulted in an upregulation of both ZEB1 mRNA and protein expression, while ZEB2 mRNA and protein expression were downregulated in the gastrocnemius muscle (Fig. 1 *A* and *B* and *SI Appendix*, Fig. S1*A*).

To investigate the possible involvement of ZEB1 and ZEB2 in the regulation of fasting-induced ROS, we selectively deleted either ZEB factor specifically in skeletal myofibers. To that effect, we first generated $Zeb1^{fl/fl}$ and $Zeb2^{fl/fl}$ mice (hereafter referred to as $Zeb1^{WT}$ and $Zeb2^{WT}$, respectively) by introducing LoxP sites in each gene. $Zeb1^{WT}$ and $Zeb2^{WT}$ were subsequently bred with the *ACTA1*-Cre-$ER^{T2\,(tg/0)}$ mouse (18)—which harbors the Cre recombinase fused to ERT2 at the start of the *ACTA1* gene, allowing for Cre recombinase expression in fully differentiated myotubes and adult differentiated myofibers—to generate $Zeb1^{\Delta SKM}$ and $Zeb2^{\Delta SKM}$ mice, respectively (*SI Appendix*, Fig. S1 *B–D*). To trigger the *ACTA1*-Cre-mediated recombination of exon 6 in *Zeb1* or exons 5 and 6 in *Zeb2*, $Zeb1^{\Delta SKM}$ and $Zeb2^{\Delta SKM}$ mice (as well as $Zeb1^{WT}$ and $Zeb2^{WT}$ mice as controls) were treated for 5 d with tamoxifen (Fig. 1*C*). *Zeb1* and *Zeb2* mRNA expression was only partially reduced in $Zeb1^{\Delta SKM}$ and $Zeb2^{\Delta SKM}$ muscles (*SI Appendix*, Fig. S1*D*) because, in addition to myofibers, ZEB1 and ZEB2 are also expressed—even at higher levels—in other cell types within skeletal muscles (e.g., satellite cells, fibroblasts, endothelial cells, immune cells) that are not subjected to Cre recombination under *ACTA1* (19, *SI Appendix*, Fig. S1*E*). Therefore, and to confirm *Zeb1* and *Zeb2* downregulation in $Zeb1^{\Delta SKM}$ and $Zeb2^{\Delta SKM}$ myofibers, respectively, primary myoblasts (that do not express *ACTA1*) isolated from the gastrocnemius of the four genotypes as well as myotubes (that do express *ACTA1*) obtained from the in vitro differentiation of the myoblasts were treated with 4-hydroxy-tamoxifen. As expected, the undifferentiated myoblasts from the four genotypes express similar levels of *Zeb1* or *Zeb2*; however, compared to $Zeb1^{WT}$ or $Zeb2^{WT}$ counterparts, *Zeb1* and *Zeb2* were reduced in $Zeb1^{\Delta SKM}$ and $Zeb2^{\Delta SKM}$ myotubes (*SI Appendix*, Fig. S1 *F* and *G*). In parallel with Fig. 1*A*, in the gastrocnemius (total muscle) of control $Zeb1^{WT}$ and $Zeb2^{WT}$ mice, fasting increased ZEB1 protein and mRNA levels and downregulated those of ZEB2 (*SI Appendix*, Fig. S1 *D* and *H*). Interestingly, and compared to the corresponding $Zeb1^{WT}$ muscles, the knockdown of *Zeb1* in fasted $Zeb1^{\Delta SKM}$ muscles, but not under fed conditions, induced an increase of *Zeb2* expression (*SI Appendix*, Fig. S1*I*). Conversely, under fed conditions, $Zeb2^{\Delta SKM}$ muscles showed increased *Zeb1* expression compared to corresponding $Zeb2^{WT}$ muscles, while no difference was observed during fasting.

The production of ROS in response to fasting were assessed in the muscles of mice of the four genotypes through five different methodological approaches. First, ROS levels were assessed by staining for dihydroethidium (DHE), a cytoplasmic blue fluorescent probe whose oxidation yields red nuclear staining. Fasting increased DHE staining in $Zeb1^{WT}$ and $Zeb2^{WT}$ mice compared to their fed counterparts (Fig. 1*D* and *SI Appendix*, Fig. S1*J*). Compared to muscles in fasted $Zeb1^{WT}$ mice, fasted $Zeb1^{\Delta SKM}$ muscles exhibited a two-fold increase in DHE staining (Fig. 1*D*). In contrast, $Zeb2^{\Delta SKM}$ myofibers did not show a similar increase in DHE staining compared to their control counterparts (Fig. 1*D*). Of note, $Zeb1^{\Delta SKM}$ muscles exhibited higher levels of ROS production during fasting compared to $Zeb1^{WT}$ muscles, while also displaying lower levels of ROS production under fed conditions, thus resulting in a greater overall increase in ROS levels (*SI Appendix*, Fig. S1*J*). Second, compared to fasted $Zeb1^{WT}$ muscles, both basally and after succinate treatment, that increases the metabolic activity of mitochondria, fasted $Zeb1^{\Delta SKM}$ muscles also exhibited higher H_2O_2 levels as measured using the Amplex™ Ultra-Red reagent (Fig. 1 *E* and *F*). In contrast, when compared to fasted $Zeb2^{WT}$ muscles, fasted $Zeb2^{\Delta SKM}$ muscles showed either similar or slightly lower H_2O_2 levels assessed by this method. Third, fasted $Zeb1^{\Delta SKM}$ muscles also exhibited a lower ratio of reduced glutathione (GSH) to oxidized glutathione (GSSG) than fasted $Zeb1^{WT}$ mice (Fig. 1*G*). Fourth, we examined ROS production levels by staining for 2′,7′-dichlorodihydrofluoresce in diacetate (CH_2-DCFDA), which becomes fluorescent upon oxidation (*SI Appendix*, Fig. S1*K*). Consistent with expectations, CH_2-DCFDA staining in fasted $Zeb1^{WT}$ and $Zeb2^{WT}$ muscles was slightly higher than in their fed counterparts. In comparison to muscles in fasted $Zeb1^{WT}$ mice, muscles in fasted $Zeb1^{\Delta SKM}$ mice exhibited increased staining intensity for CH_2-DCFDA, which becomes fluorescent upon oxidation. Conversely, fasted $Zeb2^{\Delta SKM}$ muscles displayed either similar or lower CH_2-DCFDA staining compared to their $Zeb2^{WT}$ counterparts (*SI Appendix*, Fig. S1*K*). Finally, considering that ROS can oxidize various cellular components (e.g., lipids, proteins, and nucleic acids), we utilized DNA oxidation as an indicator of oxidative stress. Fasted mice of the four genotypes were assessed for 8-hydroxydeoxyguanosine (8-OHdG) staining, the most frequently detected form of oxidized DNA. Once again, compared to fasted $Zeb1^{WT}$ muscles, fasted $Zeb1^{\Delta SKM}$ muscles showed increased staining for 8-OHdG, while 8-OHdG staining decreased in fasted $Zeb2^{\Delta SKM}$ muscles in comparison to fasted $Zeb2^{WT}$ muscles (*SI Appendix*, Fig. S1*L*). Altogether, these results suggest that *Zeb1* deletion, but not *Zeb2*, increases myofiber ROS production in response to fasting. These results suggest the existence of two divergent regulatory feedbacks between ROS and either ZEB1 or ZEB2. On the one hand, in parallel with the increase of ROS during fasting, ZEB1 expression also increases, while ZEB2 expression declines. On the other hand, *Zeb1* deletion, but not *Zeb2*, enhances myofiber ROS production in response to fasting.

Fasting-Induced Mitochondrial Damage and Muscle Atrophy Are Inhibited by ZEB1 but Potentiated by ZEB2. Mitochondria are the main source of ROS in skeletal muscle in conditions associated with muscle mass loss (6, 20). Mitochondria undergo continuous changes in size and morphology, a process known as mitochondrial dynamics, which mutually influences and is influenced by mitochondrial metabolic activity (21–23), and that regulates muscle mass and function (24).

We examined the mitochondrial morphology of fed and fasted muscles of the four genotypes by transmission electron microscopy (TEM). Intermyofibrillar mitochondria exhibited

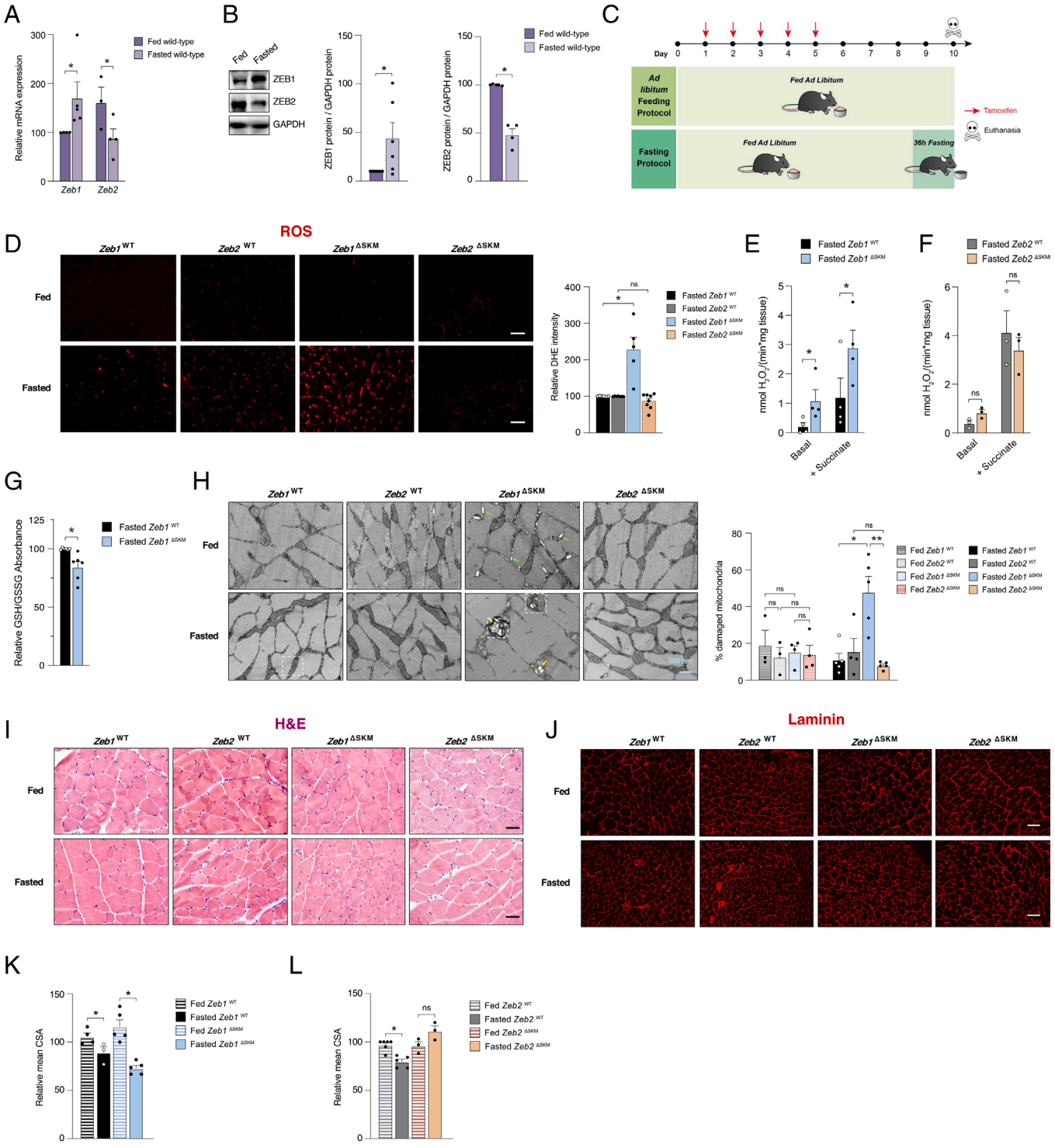

Fig. 1. ZEB1 and ZEB2 have different roles in the regulation of ROS production, mitochondrial damage, and muscle atrophy in response to fasting. (*A*) *Zeb1* and *Zeb2* mRNA levels were assessed by qRT-PCR in the gastrocnemius of 3 to 5 wild-type mice under fed and fasting conditions. *Zeb1* and *Zeb2* mRNA levels were normalized for the efficiency of their DNA primers. *Zeb1* expression under fed conditions was arbitrarily set to 100. (*B*) Lysates from the gastrocnemius of fed and fasted wild-type mice were blotted for ZEB1 (Proteintech, dilution 1/500) and ZEB2 (Abnova, M02, 1/600) along with GAPDH (14C10, 1/5,000) as a loading control. *Left*: Blots are representatives from at least 3 mice per condition. *Right:* Quantification of ZEB1 and ZEB2 protein levels relative to GAPDH levels. (*C*) Diagram of the experimental design. (*D*) ROS levels in the gastrocnemius of *Zeb1*^{WT} and *Zeb2*^{WT} mice under fed and fasting conditions were assessed by DHE staining. *Left*: Representative captures from at least six mice for each genotype and condition. (Scale bar 50 µm.) *Right*: Quantification of DHE staining using ImageJ. DHE intensity in fasted *Zeb1*^{WT} and *Zeb2*^{WT} muscles was arbitrarily set to 100. (*E*) H_2O_2 levels were measured in muscles of fasted *Zeb1*^{WT} and *Zeb1*$^{\Delta SKM}$ mice using the Amplex™ Ultra-Red reagent, both under basal conditions and after the addition of succinate. (*F*) As in (*E*), but for the fasted *Zeb2*^{WT} and *Zeb2*$^{\Delta SKM}$ muscles. (*G*) The GSH/GSSG ratio is represented as a fold change in fasted *Zeb1*$^{\Delta SKM}$ muscles relative to *Zeb1*^{WT} muscles, with data from at least six mice per genotype. (*H*) Ultrastructure of mitochondria in the gastrocnemius muscles of fed and fasted mice. *Left:* Representative TEM images. Green arrows indicate signs of a dilated sarcoplasmic reticulum, yellow asterisks highlight damaged mitochondria, and yellow arrows indicate endolysosomes. Dashed line squares are shown at a higher magnification in *SI Appendix*, Fig. S1*M*. *Right*: The percentage of "damaged mitochondria" was calculated from at least 100 mitochondria counted per mouse. (*I*) The gastrocnemius of fed and fasted mice were stained for H&E. Representative captures of at least four mice for each genotype and condition. (Scale bar: 40 µm.) (*J*) As (*I*), but sections were stained for laminin (48H-2, 1/80). (Scale bar: 100 µm.) (*K*) Mean CSA of myofibers in gastrocnemius of fed and fasted *Zeb1*^{WT} and *Zeb1*$^{\Delta SKM}$ mice. At least 100 myofibers were counted for each mouse. (*L*) As in (*K*), but for *Zeb2*^{WT} versus *Zeb2*$^{\Delta SKM}$.

a normal morphology in fed mice of the four genotypes (Fig. 1*H*). Compared to the muscles of fasted *Zeb1*^{WT} mice, fasted *Zeb1*$^{\Delta SKM}$ muscles exhibited a twofold increase in the number of mitochondria that can be categorized as "damaged mitochondria", characterized by a less electron-dense matrix, vacuolization, and/or loss of mitochondrial cristae. In contrast, fasted *Zeb2*$^{\Delta SKM}$ muscles showed nearly a 50% reduction in the number of damaged mitochondria (Fig. 1*H* and *SI Appendix*, Fig. S1*M*). Furthermore, *Zeb1*$^{\Delta SKM}$ muscles exhibited a dilatation of the sarcoplasmic reticulum (green arrows in Fig. 1*H*), along with the presence of swollen and abnormally shaped mitochondria as well as lysosome-like structures (multilamellar) that occasionally appeared partially or completely engulfed by mitochondria (yellow arrows in Fig. 1*H* and *SI Appendix*, Fig. S1*M*).

Altered mitochondrial dynamics and function can trigger muscle atrophy (3, 22–25), which is characterized by a reduction in the mean cross-sectional area (CSA) of myofibers. We explored whether the effects of ZEB1 and ZEB2 on muscle ROS production and mitochondrial integrity during fasting have an impact on muscle atrophy. The mean CSA of myofibers in the gastrocnemius muscle, a mixed muscle comprising both slow- and fast-twitch myofibers, was evaluated in fed and fasted mice of the four genotypes using hematoxylin and eosin (H&E) staining, as well as immunostaining for laminin (Fig. 1 *I* and *J*). Compared to fasted *Zeb1*^{WT} myofibers, myofibers in fasted *Zeb1*$^{\Delta SKM}$ muscles exhibited a more significant decrease in their mean CSA. However, in contrast to fasted *Zeb2*^{WT} myofibers, fasted *Zeb2*$^{\Delta SKM}$ myofibers did not experience atrophy during fasting, as evidenced by the absence of a decrease in their average CSA following fasting (Fig. 1 *K* and *L*).

Similar results were observed in the tibialis anterior muscle, which consists mainly of fast-twitch myofibers. Comparing the tibialis anterior myofibers of fasted *Zeb1*^{WT} mice to those of fasted *Zeb1*$^{\Delta SKM}$ mice, a decrease in the mean CSA was observed; in contrast, tibialis anterior myofibers of fasted *Zeb2*$^{\Delta SKM}$ mice showed an increase in their mean CSA compared to those in fasted *Zeb2*^{WT} mice (*SI Appendix*, Fig. S1 *N* and *O*).

In muscle atrophy, protein degradation takes place through the induction of a set of atrophy-related genes (referred to as atrogenes) of the ubiquitin–proteasome and the autophagy–lysosome systems (3–5). The former primarily involves the upregulation of the ubiquitin ligases Atrogin1/MAFbx (encoded by *Fbxo32*) and MuRF1 (encoded by *Trim63*) (3, 26–29). While fasting resulted in a significant upregulation of *Fbxo32* and *Trim63* mRNA expression in all four genotypes, the deletion of *Zeb1* or *Zeb2* had contrasting effects on the expression of these ubiquitin ligases. Fasted *Zeb1*$^{\Delta SKM}$ muscles showed higher mRNA levels of *Fbxo32* and *Trim63* compared to fasted *Zeb1*^{WT} muscles, whereas the fasting-induced increase in both genes was attenuated in fasted *Zeb2*$^{\Delta SKM}$ muscles compared to *Zeb2*^{WT} muscles (*SI Appendix*, Fig. S1*P*).

Collectively, these results indicate that ZEB1 and ZEB2 play opposing roles during fasting-induced muscle atrophy; while ZEB1 protected muscle from otherwise excessive atrophy in response to fasting, ZEB2 enhanced the atrophic process.

ZEB1 and ZEB2 Regulate Different Metabolic Gene Signatures in Fasted Muscles. To elucidate the mechanisms underlying the opposing phenotype of *Zeb1*$^{\Delta SKM}$ and *Zeb2*$^{\Delta SKM}$ muscles during fasting, we conducted a bulk RNA sequencing (RNAseq) of the gastrocnemius of fasted mice from the four genotypes (Fig. 2*A*). Consistent with the above results, the analysis of the RNAseq indicated that, compared to fasted *Zeb2*$^{\Delta SKM}$ muscles, fasted *Zeb1*$^{\Delta SKM}$ muscles displayed increased expression of gene signatures associated to glycolysis and muscle atrophy, and lower of genes related to oxidative phosphorylation (OxPhos) (Fig. 2*B*).

These results prompted us to study whether ZEB1 and ZEB2 play different roles in the atrophy of fibers based on their metabolic profile. Skeletal myofibers display heterogeneity in terms of their contraction speed and endurance, which corresponds to distinct metabolic profiles. Slow-twitch fibers (type I) predominantly rely on OxPhos, possess a higher mitochondrial content, and exhibit elongated mitochondria (30). In contrast, fast-twitch fibers (type IIb/x) are more glycolytic, have lower mitochondrial content, and have shorter mitochondria. Type IIa fast fibers exhibit an intermediate metabolic profile, combining aspects of both OxPhos and glycolysis. The different metabolic profiles of muscle fibers shape their responses to atrophic signals. Type IIb fibers, which are more sensitive, undergo greater protein degradation than type I and IIa fibers. As a result, during muscle atrophy, there is a relative increase in the proportion of the latter (30). Myofiber subtypes can be distinguished based on histochemical staining for myosin ATPase, with type I myofibers displaying the darkest staining, type IIa myofibers showing the lightest staining, and type IIb myofibers exhibiting an intermediate staining intensity.

We analyzed whether ZEB1 or ZEB2 expression differentially regulates the CSA and share of glycolytic and oxidative myofibers. The gastrocnemius of mice of the four genotypes under fed and fasting conditions was stained for ATPase (*SI Appendix*, Fig. S2*A*). Fasting reduced the CSA of type IIb/x myofibers in fasted *Zeb1*^{WT} and *Zeb2*^{WT} mice. However, the CSA of type I and IIa myofibers remained relatively stable during fasting (*SI Appendix*, Fig. S2 *B* and *C*). Compared to *Zeb1*^{WT} mice, fasting reduced the CSA of all types of fibers in *Zeb1*$^{\Delta SKM}$ mice but particularly of type I and IIa fibers as well as the relative share of type I fibers (*SI Appendix*, Fig. S2 *B* and *D*). However, fasting did not alter the size and share of any type of fiber in fasted *Zeb2*$^{\Delta SKM}$ mice (*SI Appendix*, Fig. S2 *C* and *E*). These findings suggest that *Zeb1* ablation renders type I and IIa fibers more susceptible to atrophy during fasting, while the absence of *Zeb2* confers resistance to fasting-induced atrophy in all fiber types, including the more sensitive glycolytic fibers.

Differential Regulation of Mitochondrial Dynamics and Autophagy Genes by ZEB1 and ZEB2. Nutrient availability alters mitochondrial dynamics (21, 22); nutrient excess and impaired OxPhos induce mitochondrial fragmentation whereas fasting and enhanced OxPhos triggers mitochondrial fusion. We investigated whether ZEB factors modulate the expression of the key components of the molecular machinery involved in mitochondrial fusion (e.g., *Mfn1*, *Mfn2*) and fission (e.g., *Drp1*, *Fis1*). No significant alterations were observed in the expression of these genes among the four genotypes under fed conditions (*SI Appendix*, Fig. S2*F*). However, compared to fasted *Zeb1*^{WT} muscles, fasted *Zeb1*$^{\Delta SKM}$ muscles exhibited upregulated mRNA and protein levels of both fusion- and fission-related genes (Fig. 2 *C* and *D* and *SI Appendix*, Fig. S2*G*). In contrast, although *Fis1* mRNA was higher in fasted *Zeb2*$^{\Delta SKM}$ muscles than in fasted *Zeb2*^{WT} muscles, the mRNA and protein expression of other fusion and fission genes was similar in fasted *Zeb2*^{WT} and *Zeb2*$^{\Delta SKM}$ muscles.

In addition to the ubiquitin-proteasome system, a second catabolic mechanism involved in protein degradation during muscle atrophy is the autophagy–lysosome system (5, 29, reviewed in refs. 3 and 31). Elimination through autophagy of damaged organelles, including mitochondria, and ubiquitinated proteins plays a crucial role in maintaining muscle homeostasis and its inhibition enhances muscle loss in response to atrophic signals (3, 31). The analysis of RNAseq data showed that fasted *Zeb1*$^{\Delta SKM}$ muscles exhibited lower expression of autophagy gene signatures compared to *Zeb2*$^{\Delta SKM}$ counterparts (Fig. 2*E*). The eventual fusion of autophagosomes with lysosomes involves components of the ATG8 family (LC3

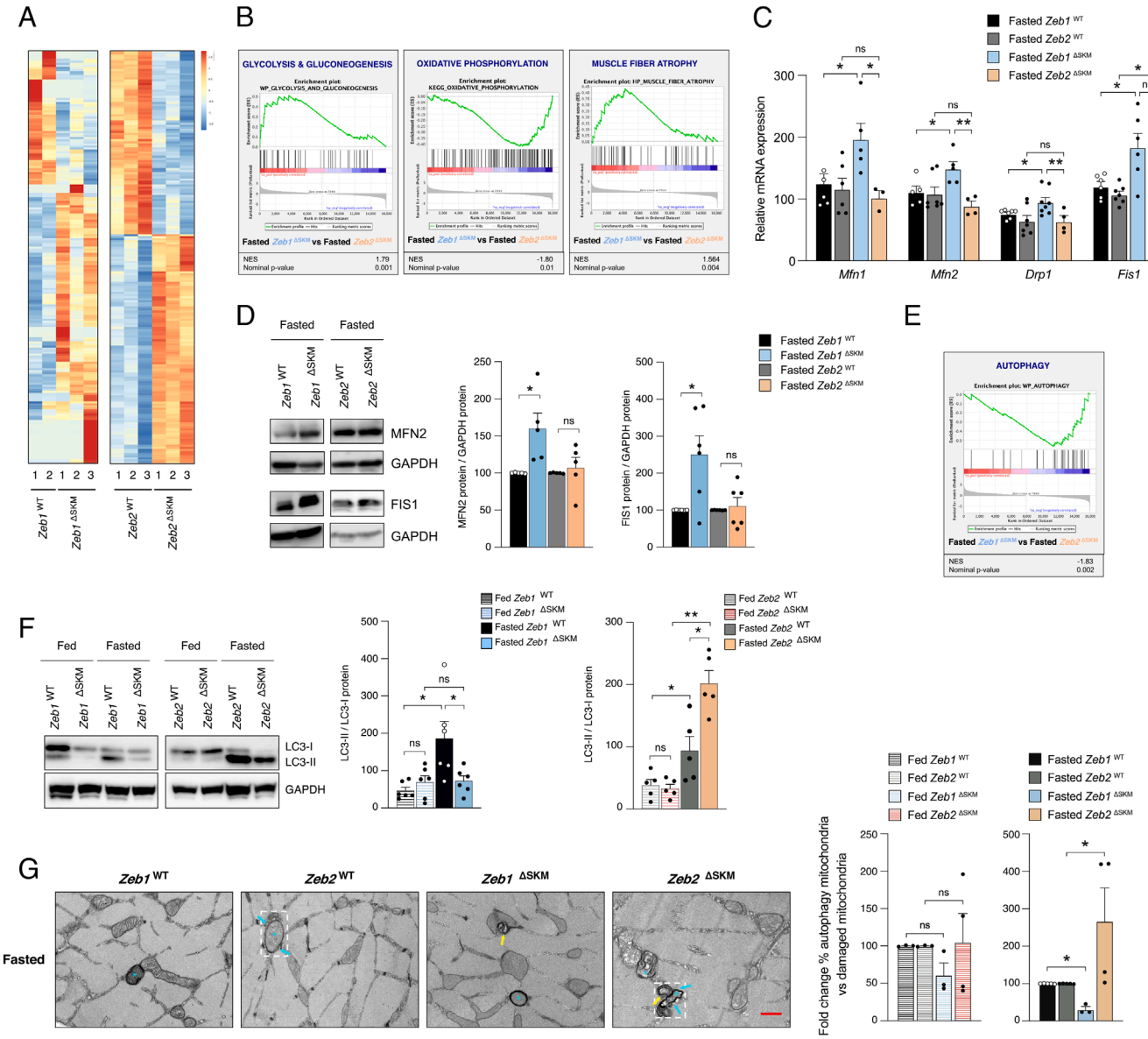

Fig. 2. ZEB1 and ZEB2 differentially regulate genes involved in muscle atrophy, mitochondrial dynamics, and autophagy. (*A*) Heatmap of the top 200 DEGs in the gastrocnemius of fasted *Zeb1*$^{\Delta SKM}$ muscles versus fasted *Zeb1*^{WT} muscles and fasted *Zeb2*$^{\Delta SKM}$ muscles versus fasted *Zeb2*^{WT} muscles. (*B*) GSEA plots for gene signatures of glycolysis, OxPhos, and muscle atrophy in fasted *Zeb1*$^{\Delta SKM}$ mice versus fasted *Zeb2*$^{\Delta SKM}$ mice. (*C*) Relative mRNA expression of *Mfn1, Mfn2, Drp1,* and *Fis1* in the gastrocnemius of fasted mice of the four genotypes. (*D*) Gastrocnemius lysates from fasted mice of the four genotypes were blotted for MFN2 (F5, 1/500), FIS1 (B5, 1/500), and GAPDH (14C10, 1/5000). *Left*: Blots are representative from at least five independent experiments. *Right:* Quantification of the MFN2 or FIS1 protein levels relative to GAPDH. (*E*) GSEA plot for an autophagy gene signature in fasted *Zeb1*$^{\Delta SKM}$ mice compared to fasted *Zeb2*$^{\Delta SKM}$ mice. (*F*) Gastrocnemius lysates from fed and fasted mice of the four genotypes were blotted for LC3 (14600-1-AP, 1/1,000) and GAPDH. *Left*: Representative blots of at least five independent experiments. *Right:* Ratio between LC3-II and LC3-I. (*G*) Ultrastructure captures of gastrocnemius from fasted mice of the four genotypes. *Left:* Representative TEM pictures highlighting damaged mitochondria (yellow arrows), signs of autophagy (blue asterisks), and double membranes (blue arrows). (Scale bar: 500 nm.) *Right*: Quantification of the number of mitochondria with signs of autophagy relative to the total number of damaged mitochondria.

and GABARAP) (3, 31). We found that the ratio between the lipidated form of LC3 (LC3-II, an autophagosomal marker) and its nonlipidated form (LC3-I) was lower in fasted *Zeb1*$^{\Delta SKM}$ muscles than in fasted *Zeb1*^{WT} counterparts; in contrast, fasted *Zeb2*$^{\Delta SKM}$ muscles exhibited a higher LC3-II/LC3-I ratio than fasted *Zeb2*^{WT} muscles (Fig. 2*F* and *SI Appendix*, Fig. S2*H*). Fasted *Zeb1*$^{\Delta SKM}$ muscles also exhibited reduced levels of autophagic bodies compared to fasted *Zeb1*^{WT} muscles, while fasted *Zeb2*$^{\Delta SKM}$ muscles showed a significant increase, more than doubling the levels of autophagic bodies in fasted *Zeb2*^{WT} muscles (Fig. 2*G* and *SI Appendix*, Fig. S2*I*), results that can contribute to explain their respective enhanced and reduced muscle atrophy upon fasting.

ZEB1 Activates Mitochondrial ETC Complexes III and IV, while ZEB2 Inhibits ETC Complex IV. We then examined the impact of ZEB1 and ZEB2 on mitochondrial function using high-resolution mitochondrial respirometry. Isolated muscles from the four genotypes were analyzed under both fed and fasting conditions using a two-chamber Oxygraph-2k system. Oxygen consumption by mitochondrial ETC complexes I to IV (CI to CIV) was determined by titration with their respective inhibitors (32). Under fed conditions, except for a lower activity of CIV in *Zeb1*$^{\Delta SKM}$ muscles, no significant differences were observed in the oxygen flux of all ETC complexes among the four genotypes (*SI Appendix*, Fig. S3 *A* and *B*). Under fasting conditions, oxygen consumption by CIII

and CIV in muscles from fasted *Zeb1*$^{\Delta SKM}$ mice was approximately halved compared to fasted *Zeb1*^{WT} muscles, while fasted *Zeb2*$^{\Delta SKM}$ mice showed an elevated oxygen flux specifically in CIV relative to *Zeb2*^{WT} muscles (Fig. 3 *A* and *B*).

We subsequently measured the activity of citrate synthase (CS), which is the first enzyme of the tricarboxylic acid cycle and a mitochondrial matrix protein. Compared to fasted *Zeb1*^{WT} muscles, *Zeb1*$^{\Delta SKM}$ muscles did not show a significant change in CS activity. However, fasted *Zeb2*$^{\Delta SKM}$ muscles exhibited higher CS activity than their *Zeb2*^{WT} counterparts (*SI Appendix*, Fig. S3*C*). Next, we measured the joint enzymatic activity of CII and CIII relative to CS activity to account for tissue variability. In fasted *Zeb1*$^{\Delta SKM}$ muscles, the intrinsic CII+CIII activity was lower than in fasted *Zeb1*^{WT} muscles (Fig. 3*C*).

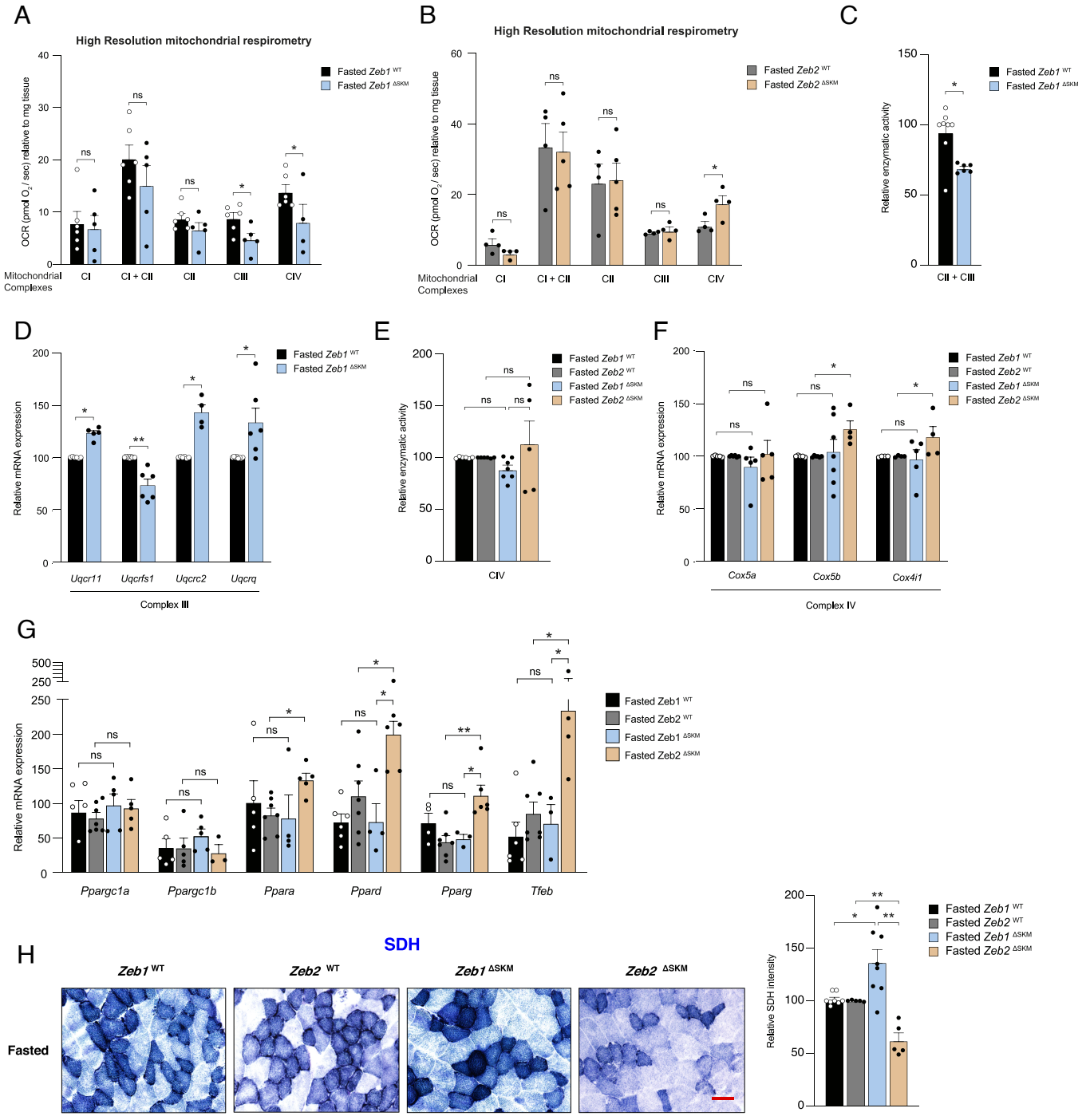

Fig. 3. ZEB1 activates mitochondrial ETC complexes III and IV, while ZEB2 inhibits ETC complex IV. (*A*) High-resolution respirometry of permeabilized gastrocnemius muscles from fasted *Zeb1*$^{\Delta SKM}$ mice compared to those of fasted *Zeb1*^{WT} mice. (*B*) As in (*A*), but for fasted *Zeb2*$^{\Delta SKM}$ and *Zeb2*^{WT} mice. (*C*) The enzymatic activity of CII+CIII in the gastrocnemius of fasted *Zeb1*$^{\Delta SKM}$ mice compared to fasted *Zeb1*^{WT} mice. Mitochondrial complex activity was normalized to CS activity. The absorbance of fasted *Zeb1*^{WT} muscles was arbitrarily set to 100. (*D*) Relative mRNA expression of *Uqcr11*, *Uqcrfs1*, *Uqcrc2*, and *Uqcrq* in the gastrocnemius muscles of fasted *Zeb1*^{WT} and *Zeb1*$^{\Delta SKM}$ mice. mRNA levels in fasted *Zeb1*^{WT} muscles were arbitrarily set to 100. (*E*) CIV activity in fasted *Zeb1*$^{\Delta SKM}$ and *Zeb2*$^{\Delta SKM}$ mice is presented relative to that in fasted *Zeb1*^{WT} and *Zeb2*^{WT} mice, which were arbitrarily set to 100. (*F*) Relative mRNA expression of *Cox5a, Cox5b*, and *Cox4i1* in the gastrocnemius of fasted mice of the four genotypes. (*G*) Relative mRNA expression of *Ppargc1a, Ppargc1b, Ppara, Ppard, Pparg,* and *Tfeb* in the gastrocnemius of fasted mice of the four genotypes. (*H*) SDH staining in the gastrocnemius muscles of fasted mice of the four genotypes. *Left*: Representative pictures. (Scale bar: 100 μm.) *Right*: Mean relative intensity of total SDH. At least five images at 20× magnification per mouse were quantified.

Proteins in the mitochondrial ETC are encoded by genes in both the nuclear (nDNA) and mitochondrial (mtDNA) DNA. As ZEB1 and ZEB2 are nuclear transcription factors, we focused our analysis on selected nDNA-encoded CIII genes. Under fed conditions, we observed similar expression levels of *Uqcr11, Uqcrc2, Uqcrq*, and *Uqcrfs1* in both *Zeb1*^{WT} and *Zeb1*$^{\Delta SKM}$ muscles (*SI Appendix*, Fig. S3*D*). However, in fasting, the expression of *Uqcr11, Uqcrc2*, and *Uqcrq* was upregulated, while *Uqcrfs1* was downregulated in *Zeb1*$^{\Delta SKM}$ muscles compared to *Zeb1*^{WT} counterparts (Fig. 3*D*).

We found no significant difference in CIV activity relative to CS activity among the fasted muscles of the four genotypes (Fig. 3*E*). We also analyzed the expression of several nDNA-encoded CIV enzymes, namely *Cox5a, Cox5b*, and *Cox4i1*. While there were no differences in the expression of these CIV genes in the muscles of fed mice across the four genotypes (*SI Appendix*, Fig. S3*E*), consistent with Fig. 3*B*, fasted *Zeb2*$^{\Delta SKM}$ muscles showed higher levels of *Cox5b* and *Cox4i1* compared to fasted *Zeb2*^{WT} mice (Fig. 3*F*). Altogether, these data suggest that during fasting, ZEB1 increases the activity of CIII and CIV, while ZEB2 inhibits the activity of CIV.

Mitochondrial homeostasis relies on a delicate equilibrium between the regulation of mitochondrial dynamics and biogenesis and the clearance of damaged mitochondria through mitophagy to maintain mitochondrial number, size, and integrity (22). Analysis of TOMM20 protein expression, a component of the outer mitochondrial membrane, in the four genotypes under fed and fasting conditions, indicated that TOMM20 levels were higher in fasted *Zeb1*$^{\Delta SKM}$ muscles compared to fasted *Zeb1*^{WT} mice. However, no significant change in TOMM20 expression was observed in fasted *Zeb2*$^{\Delta SKM}$ muscles compared to their corresponding fasted *Zeb2*^{WT} mice (*SI Appendix*, Fig. S3 *F* and *G*). We also investigated the expression of a panel of genes associated with mitochondrial biogenesis (including *Ppargc1a, Ppargc1b, Ppara, Ppard, Pparg*, and *Tfeb*) in the gastrocnemius muscles of fed and fasted mice from the four genotypes. We observed no significant differences in the expression of these genes among the four genotypes under fed conditions (*SI Appendix*, Fig. S3*H*). In fasting, the expression of these genes was not significantly affected by the deletion of *Zeb1*. However, fasted *Zeb2*$^{\Delta SKM}$ muscles showed increased levels of *Ppara, Ppard, Pparg*, and *Tfeb* compared to fasted *Zeb2*^{WT} muscles (Fig. 3*G*).

Complex II, which consists of the two largest subunits of succinate dehydrogenase (SDH), is the only ETC complex entirely encoded by nDNA. Thus, SDH staining can be used to evaluate myofiber type and mitochondrial content without being influenced by changes in mtDNA. The average staining intensity of SDH was similar in the fed muscles of all four genotypes (*SI Appendix*, Fig. S3*I*). However, fasting led to increased SDH staining in *Zeb1*$^{\Delta SKM}$ muscles compared to fasted *Zeb1*^{WT} muscles, while it was halved in *Zeb2*$^{\Delta SKM}$ mice compared to *Zeb2*^{WT} mice (Fig. 3*H*).

NRF2 Expression and Its Downstream Antioxidant Response Depend on ZEB1 and Is Inhibited by ZEB2. We investigated whether the diverging levels of ROS in fasted *Zeb1*$^{\Delta SKM}$ and *Zeb2*$^{\Delta SKM}$ mice were due to differential regulation of the cellular antioxidant response. Central to this antioxidant response is the transcription factor NRF2 (encoded by *Nfe2l2*) (8, 10). Under fed conditions, no significant differences were detected in *Nfe2l2* mRNA levels between fed *Zeb1*^{WT} and *Zeb1*$^{\Delta SKM}$ mice, whereas *Zeb2*$^{\Delta SKM}$ muscles express higher *Nfe2l2* mRNA levels than *Zeb2*^{WT} mice (Fig. 4*A*). However, in a reverse pattern with their respective ROS levels, the gastrocnemius muscles of fasted *Zeb1*$^{\Delta SKM}$ mice showed lower expression of both NRF2 mRNA and protein compared to fasted *Zeb1*^{WT}, while the gastrocnemius muscles of fasted *Zeb2*$^{\Delta SKM}$ mice exhibited higher levels of NRF2 mRNA and protein compared to fasted *Zeb2*^{WT} mice (Fig. 4 *A* and *B* and *SI Appendix*, Fig. S4*A*). Similar results were found in the tibialis anterior of fasted mice of the four genotypes (*SI Appendix*, Fig. S4*B*). As for *Nfe2l2, Zeb1*$^{\Delta SKM}$ mice showed lower mRNA expression of the related *Nrf1* factor (*SI Appendix*, Fig. S4*C*).

The reverse regulation of NRF2 expression in fasted *Zeb1*$^{\Delta SKM}$ and *Zeb2*$^{\Delta SKM}$ muscles was not associated with differential expression of KEAP1 (*SI Appendix*, Fig. S4 *D* and *E*). Despite an increase in both mRNA and protein levels of KEAP1 during fasting in all genotypes compared to fed muscles, no differences were observed between the fasted muscles of the four genotypes. *Zeb2*$^{\Delta SKM}$ muscles exhibited increased nuclear localization of NRF2 compared to fasted *Zeb2*^{WT} muscles, while fasted *Zeb1*$^{\Delta SKM}$ muscles showed decreased NRF2-positive nuclei compared to fasted *Zeb1*^{WT} counterparts (Fig. 4 *C* and *D* and *SI Appendix*, Fig. S4*F*).

Analysis of our RNAseq data indicated that direct target genes of NRF2 were expressed at higher levels in the muscles of fasted *Zeb2*$^{\Delta SKM}$ mice compared to fasted *Zeb1*$^{\Delta SKM}$ mice (Fig. 4*E*). The regulation of NRF2 downstream genes by ZEB1 and ZEB2 was investigated using qRT-PCR for *Nqo1, Hmox1, Gclm, Txn1*, and *Gsr*. Albeit to a different extent among genes, gene expression decreased in fasted *Zeb1*$^{\Delta SKM}$ mice and increased in fasted *Zeb2*$^{\Delta SKM}$ mice compared to *Zeb1*^{WT} and *Zeb2*^{WT} muscles, respectively (Fig. 4*F*). A similar result was observed for *Hmox1* in the tibialis anterior muscle of fasted *Zeb1*$^{\Delta SKM}$ mice compared to fasted *Zeb2*$^{\Delta SKM}$ mice (*SI Appendix*, Fig. S4*G*).

These results prompted us to explore whether ZEB factors regulate NRF2 expression at the transcriptional level. ZEB1 and ZEB2 bind to similar sequences in the regulatory regions of their target genes whose expression they activate or repress depending on the cofactors they recruit (34 to 38). Analysis of the mouse *Nfe2l2* promoter identified six consensus binding sites for ZEB1/ZEB2 within its first 1.2 kb (*SI Appendix*, Fig. S4*H*). The ability of ZEB1 and ZEB2 to regulate the transcriptional activity of the *Nfe2l2* promoter was examined upon their knockdown or overexpression. Compared to a control nontargeting siRNA, siRNAs targeting *Zeb1* (si*Zeb1*-A and si*Zeb1*-B) downregulated *Nfe2l2* promoter activity, while siRNAs against *Zeb2* (si*Zeb2*-A and si*Zeb2*-B) upregulated it (Fig. 4*G* and *SI Appendix*, Fig. S4*I*). Conversely, *Zeb1* overexpression led to the activation of *Nfe2l2* promoter transcription, whereas the overexpression of *Zeb2* repressed it (Fig. 4*H*). These results indicate that both ZEB factors can regulate *Nfe2l2* transcription and led us to explore the in vivo binding of ZEB1 and/or ZEB2 to the *Nfe2l2* promoter through chromatin immunoprecipitation (ChIP) assays. Antibodies against either ZEB1 or ZEB2, but not their corresponding control matched species IgG, immunoprecipitated a region of the *Nfe2l2* promoter containing a ZEB-binding site in atrophic C2C12 myotubes (Fig. 4*I*). The binding of both ZEB1 and ZEB2 to the same sites in the *Nfe2l2* promoter suggests that they may be playing their opposing roles at different times during the atrophic process (see below in *Discussion*).

Exogenous NRF2 Induction Rescues the Phenotype of *Zeb1*-Deficient Muscles. To determine whether the phenotype of fasted *Zeb1*$^{\Delta SKM}$ mice is due to their reduced NRF2 expression, we rescued NRF2 levels in these mice in a ZEB1-independent manner using the synthetic triterpenoid 1[2-cyano-3,12-dioxooleana-1,9(11)-dien-28-oyl] trifluoro-ethylamide (CDDO-TFEA) (7, 33) (Fig. 5*A*). CDDO-TFEA treatment did not affect ZEB1 levels but effectively restored the expression of NRF2 and selected NRF2 downstream genes in fasted *Zeb1*$^{\Delta SKM}$ muscles, bringing

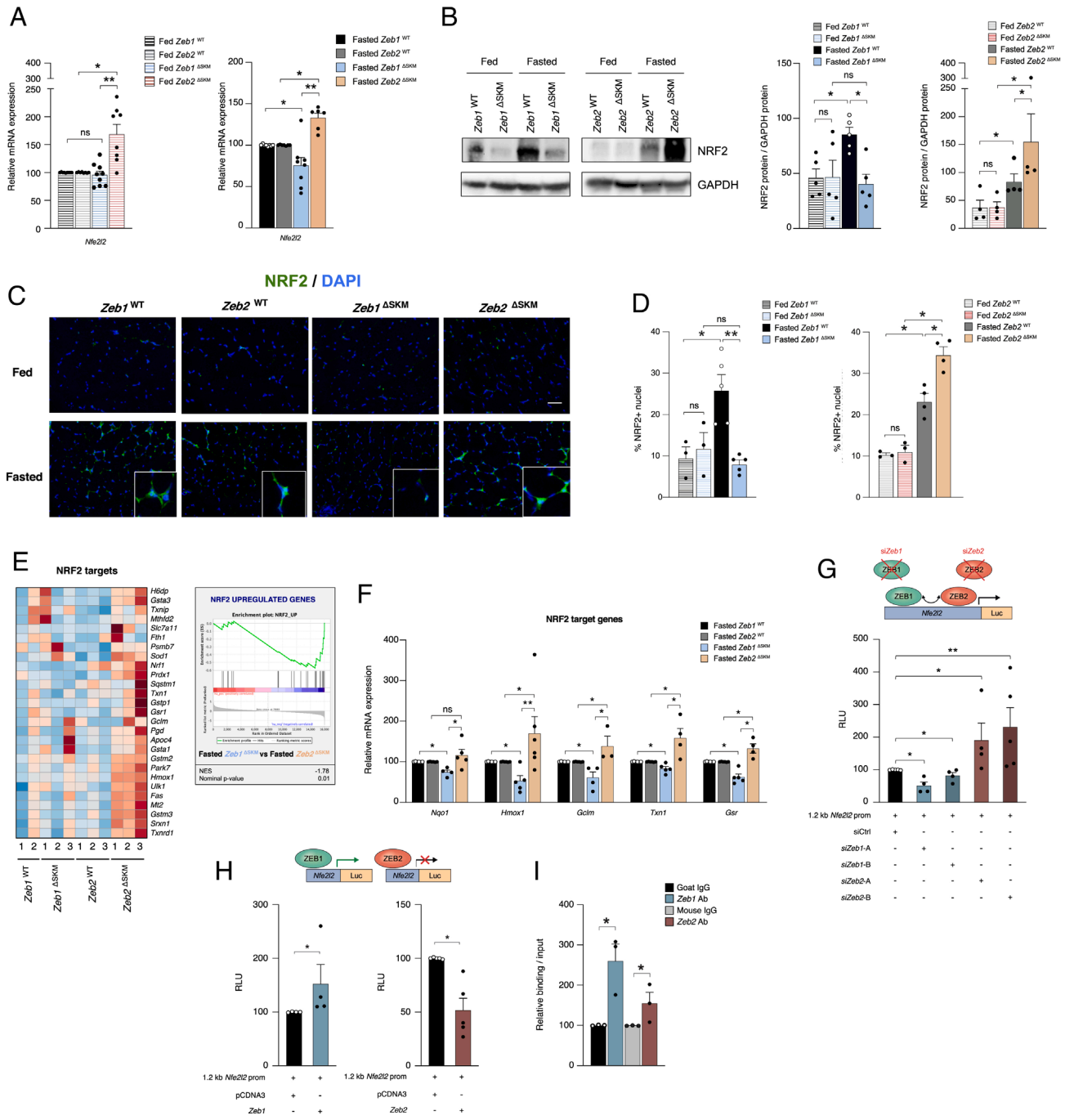

Fig. 4. NRF2 expression and the adaptive NRF2-driven antioxidant response to fasting depend on ZEB1 and is inhibited by ZEB2. (*A*) Relative *Nfe2l2* mRNA expression in the gastrocnemius of fed and fasted mice from the four genotypes. In each treatment, *Zeb1*^{WT} and *Zeb2*^{WT} mRNA levels were arbitrarily set to 100. (*B*) Gastrocnemius lysates from fed and fasted muscles of the four genotypes were blotted for NRF2 (1F2, 1/500) and GAPDH (14C10, 1/5,000). *Left:* Representative blots are shown. *Right:* Quantification of NRF2 protein levels relative to GAPDH in at least four independent experiments. (*C*) NRF2 (1F2, 1/700) immunostaining along with DAPI in fed and fasted gastrocnemius of the four genotypes. Representative captures from at least five mice per genotype and condition. Insets with higher magnification for the fasting condition. (Scale bar: 50 μm.) (*D*) Quantification of NRF2-positive nuclei in the four genotypes under fed and fasted conditions, presented as the percentage of NRF2-positive nuclei versus the total number of nuclei per field. Mean values are based on at least three mice, with at least 100 nuclei counted per mouse. (*E*) Expression of NRF2 target genes in fasted muscles of the four genotypes. *Left*: Heatmap of NRF2 target genes in fasted muscles of the four genotypes. *Right*: GSEA plots for NRF2 target genes in fasted *Zeb1*$^{\Delta SKM}$ gastrocnemius relative to fasted *Zeb2*$^{\Delta SKM}$ counterparts. (*F*) Relative mRNA expression of *Nqo1*, *Hmox1*, *Gclm*, *Txn1,* and *Gsr* in fasted gastrocnemius of the four genotypes. mRNA levels in fasted *Zeb1*$^{\Delta SKM}$ and *Zeb2*$^{\Delta SKM}$ mice are represented relative to those of fasted *Zeb1*^{WT} and *Zeb2*^{WT} muscles, respectively, set to 100. (*G*) Transcriptional activity of the mouse *Nfe2l2* promoter following knockdown of either *Zeb1* or *Zeb2*. A total of 0.43 μg of a 1.2-kb mouse luciferase reporter of the *Nfe2l2* promoter were transfected in C2C12 myoblasts along with 50 nM of either a siRNA control (siCtrl) or specific siRNAs against *Zeb1* (si*Zeb1*-A, si*Zeb1*-B) or *Zeb2* (si*Zeb2*-A, si*Zeb2*-B). The activity of the luciferase reporter with siCtrl was arbitrarily set to 100. Data represent the average of at least three independent experiments. (*H*) As in (*G*), but the *Nfe2l2* luciferase reporter was cotransfected in atrophic C2C12 myotubes with either 0.06 μg of the empty expression vector or 0.10 μg of an expression vector for *Zeb1* (*Left*) or, alternatively, with 0.17 μg of the empty expression vector or 0.30 μg of an expression vector for *Zeb2* (*Right*). The condition with the *Nfe2l2* luciferase reporter plus the empty vector was set to 100. Data are the average of at least three independent experiments. (*I*) ZEB1 and ZEB2 binding to the *Nfe2l2* promoter in atrophic C2C12 myotubes was determined by ChIP.

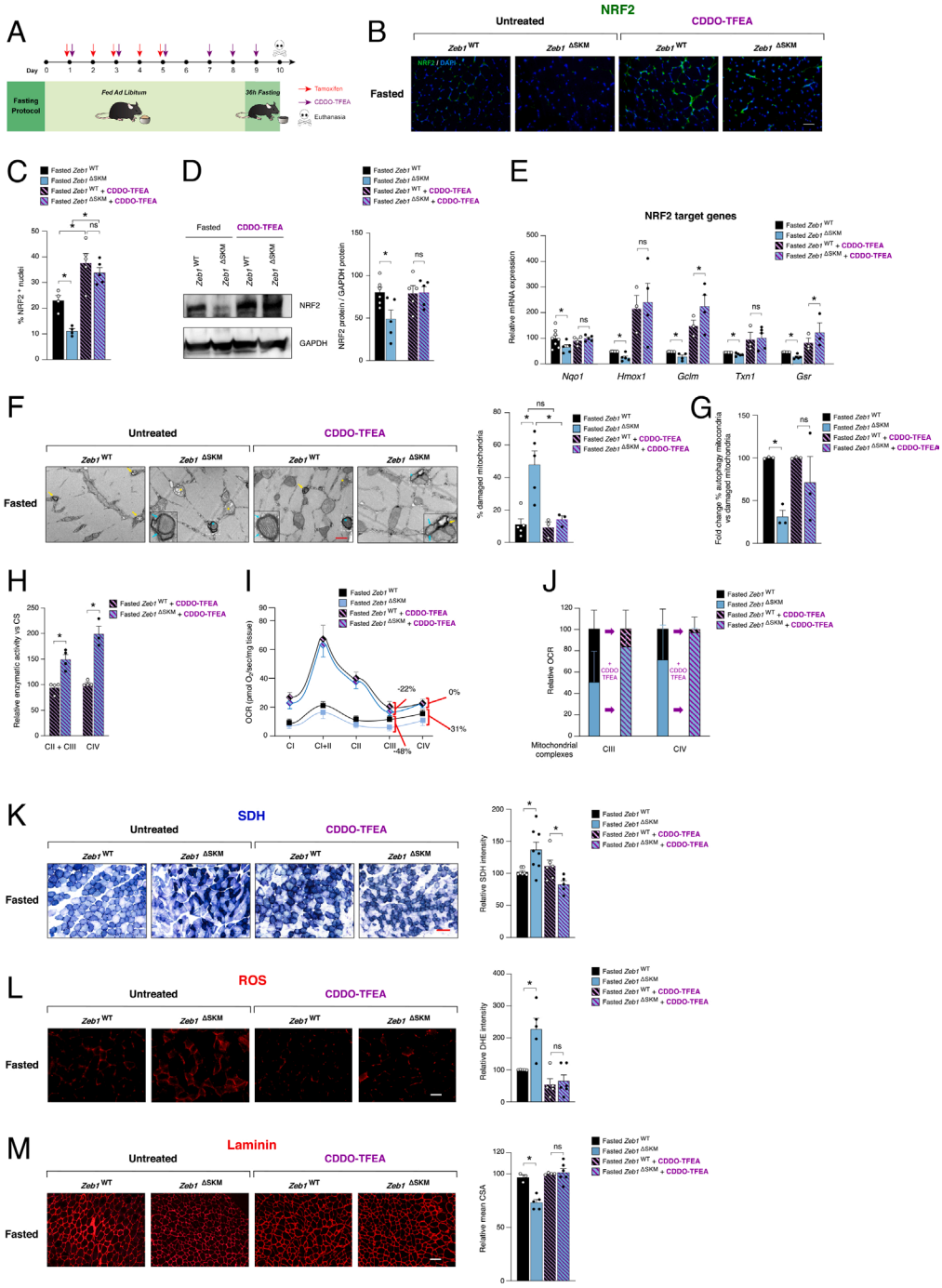

Fig. 5. Exogenous induction of NRF2 rescues the phenotype in *Zeb1*-deficient muscles. (*A*) Experimental design of fasted *Zeb1*^{WT} and *Zeb1*$^{\Delta SKM}$ mice either untreated or treated with CDDO-TFEA. (*B*) Immunostaining for NRF2 (1F2, 1/700) along with DAPI in the gastrocnemius of fasted *Zeb1*^{WT} and *Zeb1*$^{\Delta SKM}$ mice either untreated or treated with CDDO-TFEA. Captures are representative of at least four mice per genotype and condition. (Scale bar: 50 µm.) (*C*) NRF2-positive nuclei per field were quantified in fasted *Zeb1*^{WT} and *Zeb1*$^{\Delta SKM}$ mice, with or without CDDO-TFEA treatment. Mean values are based on at least three mice, with at least 100 nuclei counted per mouse. (*D*) Gastrocnemius lysates from fasted *Zeb1*^{WT} and *Zeb1*$^{\Delta SKM}$ mice, either untreated and treated with CDDO-TFEA, were blotted for NRF2 (1F2, 1/500) and GAPDH (14C10, 1/5,000). *Left*: Representative blots. *Right*: Quantification of NRF2 protein levels relative to GAPDH protein levels in at least five independent experiments. (*E*) mRNA expression of *Nqo1*, *Hmox1*, *Gclm*, *Txn1*, and *Gsr* in the gastrocnemius of fasted *Zeb1*^{WT} and *Zeb1*$^{\Delta SKM}$ mice, either with or without CDDO-TFEA treatment. (*F*) As in (*B*), ultrastructure evaluation of mitochondria. Damaged mitochondria (yellow asterisks), endolysosomes (yellow arrows), signs of autophagy (blue asterisks), and the presence of double-membrane (blue arrows) are highlighted. *Left*: Representative TEM captures. *Right:* The percentage of damaged mitochondria was calculated from at least three mice per genotype and treatment group, with at least 100 mitochondria counted for each mouse. (*G*) As in the *Right* panel of (*F*), the percentage of mitochondria undergoing autophagy was calculated from the total number of damaged mitochondria. (*H*) CII+CIII and CIV enzymatic activities in the gastrocnemius of fasted *Zeb1*^{WT} and *Zeb1*$^{\Delta SKM}$ mice, either untreated or treated with CDDO-TFEA. CII+CIII and CIV activities were normalized to CS activity. The relative absorbance of CDDO-TFEA-treated *Zeb1*^{WT} mice was set to 100. At least three mice per genotype and condition were assessed. (*I*) The oxygen consumption rate (OCR) of the gastrocnemius fibers of fasted *Zeb1*^{WT} and *Zeb1*$^{\Delta SKM}$ mice, either untreated or treated with CDDO-TFEA, was assessed by high-resolution respirometry. At least four mice per genotype and treatment group were assessed. (*J*) As in (*I*), but CIII and CIV activities were compared in fasted *Zeb1*^{WT} versus *Zeb1*$^{\Delta SKM}$ fibers from mice with and without CDDO-TFEA treatment. (*K*) SDH staining of the gastrocnemius of fasted *Zeb1*^{WT} and *Zeb1*$^{\Delta SKM}$ mice, either untreated or treated with CDDO-TFEA. *Left*: Representative captures. (Scale bar 100 µm.) *Right*: quantification of SDH staining using ImageJ software. At least five images at 20× magnification per mouse were assessed. SDH mean intensity in untreated *Zeb1*^{WT} mice was set to 100. (*L*) As in (*K*), but for DHE staining. (Scale bar 100 µm.) (*M*) Gastrocnemius myofiber CSA analysis in fasted mice of the four genotypes, either untreated or treated with CDDO-TFEA. *Left*: Representative muscle sections stained for laminin (48H-2, 1/80). (Scale bar 100 µm.) *Right*: Quantification of the mean CSA.

them to similar or higher levels compared to *Zeb1*^{WT} muscles (Fig. 5 *B–E* and *SI Appendix*, Fig. S5 *A–C*).

Administration of CDDO-TFEA reduced the number of damaged mitochondria and mitochondria undergoing autophagy in fasted *Zeb1*$^{\Delta SKM}$ mice to values comparable to those in fasted *Zeb1*^{WT} mice (Fig. 5 *F* and *G* and *SI Appendix*, Fig. S5*D*). CDDO-TFEA restored the lower activity of CII+CIII and CIV in fasted *Zeb1*$^{\Delta SKM}$ muscles to similar levels—and in some instances even surpassed them— than in fasted *Zeb1*^{WT} muscles (Fig. 5 *H–J*). Similarly, CDDO-TFEA treatment of fasted *Zeb1*$^{\Delta SKM}$ mice reverted their more intense SDH staining compared to *Zeb1*^{WT} (Fig. 5*K*). These effects were independent of changes in mitochondrial content, as evidenced by comparable TOMM20 expression and CS activity in both untreated and CDDO-TFEA-treated mice (*SI Appendix*, Fig. S5 *E* and *F*).

The observed increase in ROS levels in the muscles of fasted *Zeb1*$^{\Delta SKM}$ mice was linked to their lower NRF2 expression as CDDO-TFEA reduced ROS levels in these mice to levels similar to those in fasted *Zeb1*^{WT} mice (Fig. 5*L*). Finally, CDDO-TFEA also reversed the increased muscle atrophy in fasted *Zeb1*$^{\Delta SKM}$ mice (Fig. 5*M*).

Taken together, these findings suggest that the altered phenotype exhibited by fasted *Zeb1*$^{\Delta SKM}$ muscles was due, at least to a significant extent, to a reduced expression of the adaptive antioxidant response regulated by NRF2.

Discussion

ROS performs important homeostatic roles, but oxidative stress is both a cause and a consequence of multiple diseases (7, 10). Consequently, ROS and NRF2 levels must be tightly and constantly modulated. Here, we found that ZEB1 and ZEB2 regulate the adaptive antioxidant response to fasting in skeletal muscle in opposite directions (see *SI Appendix*, *Supplementary Discussion* and graphical summary in Fig. 6).

Although approximately half of the atrogenes upregulated during muscle atrophy are induced by FOXO3, many genes involved in the adaptive antioxidant response, including NRF2 itself, are induced through a FOXO3-independent mechanism (29). Apart from inhibiting atrogene expression by antagonizing FOXO3 transcriptional activity (34), the findings here indicate that ZEB1 protects myofibers from mitochondrial damage and otherwise excessive ROS levels and muscle atrophy by transcriptionally activating the *Nfe2l2* promoter and upregulating NRF2 target genes. Conversely, ZEB2 enhances muscle atrophy by transcriptionally repressing *Nfe2l2* and downregulating its downstream antioxidant program (*SI Appendix*, *Supplementary Discussion*).

ZEB1 and ZEB2 bind to similar DNA sequences in their target genes (35, 36) and we found that both ZEB factors bind to the *Nfe2l2* promoter in atrophic C2C12 myotubes in ChIP assays. It is safe to assume that among atrophic C2C12 myotubes in culture or fasted myofibers in vivo, not all cells are in the same stage of the atrophic process. The inverse expression of ZEB1 and ZEB2 in fed and fasted muscles, as well as the repression of ZEB2 by ZEB1 in fasted muscles, leads us to hypothesize that the results in the ChIP assay are due to ZEB2 and ZEB1 binding to the *Nfe2l2* promoter at earlier and later stages of the atrophic process, respectively. At later stages, ZEB1 upregulation and repression of ZEB2 expression would allow ZEB1 to induce NRF2 and its antioxidant pathway to counter ROS levels (*SI Appendix*, *Supplementary Discussion*).

In summary, the study identified a mechanism that modulates the NRF2-driven adaptive antioxidant response. Therapeutic approaches aimed at upregulating the expression or function of ZEB1 and/or downregulating that of ZEB2 can be used in pathological conditions in which supraphysiological levels of ROS are an underlying factor.

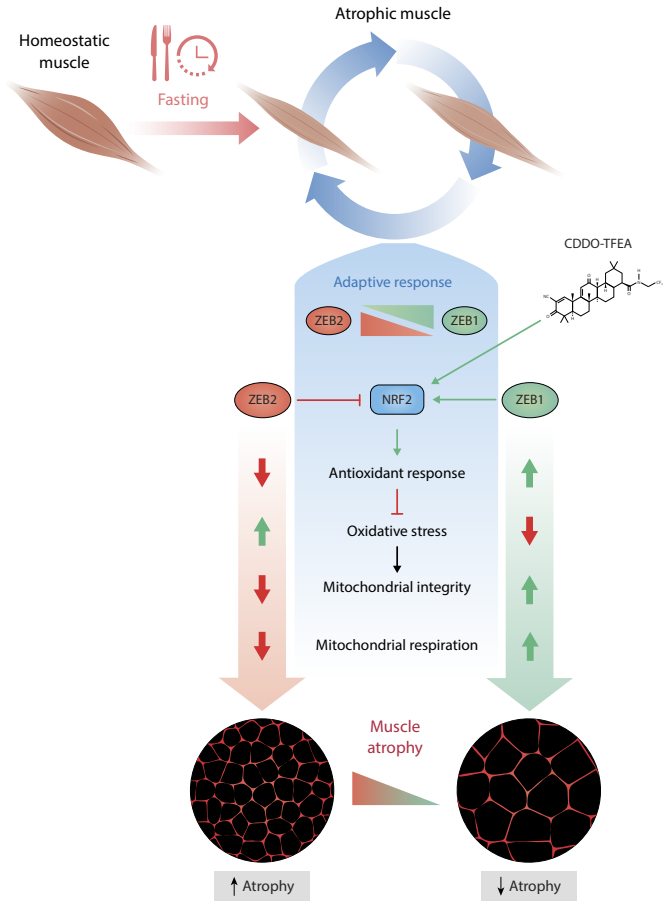

Fig. 6. Graphical summary. The NRF2-driven antioxidant response to fasting depends on ZEB1 and is inhibited by ZEB2.

Materials and Methods

Detailed methods are described in *SI Appendix*, *Materials and Methods*.

Mouse Models. To generate *Zeb1*$^{\Delta SKM}$ and *Zeb2*$^{\Delta SKM}$ mice, *Zeb1*^{WT} and *Zeb2*^{WT} mice were crossed with *ACTA1*-Cre-ER$^{T2\,(tg/0)}$ mouse. Two-to-three months-old mice of the four genotypes and both sexes were injected intraperitoneally daily for 5 d with tamoxifen (Sigma-Aldrich, St. Louis, MO, USA) and then divided in two cohorts; one was deprived of food but free access to water (fasting protocol) for 36 additional hours, and the other was allowed to feed and drink water ad libitum (fed protocol).

Determination of ROS and Oxidative Stress. ROS production and the oxidation of macromolecules was assessed by staining for DHE, CH_2-DCFDA and 8-OHdG, Amplex® Ultra-Red, and the determination of GSH/GSSG ratio.

Histochemistry, Immunostaining, and Assessment of Myofiber CSA. First, 8-µm cryosections were fixed and stained with H&E or incubated with the corresponding primary and HRP-conjugated secondary antibodies as described elsewhere (19, 34). Histochemistry visualization of SDH and ATPase activity was conducted by incubation of muscle cryosections with their respective staining solutions. Then, myofiber CSA and SDH and ATPase staining were assessed using ImageJ software (NIH, Bethesda, MD) as described elsewhere (19, 32, 34) and in *SI Appendix*, *Materials and Methods*.

Mitochondria Ultrastructure and Determination of Mitochondrial Complexes Activity. Ultrastructure analysis of muscle mitochondria was conducted by TEM, while high-resolution respirometry and the activity of individual mitochondrial complexes were determined as described in ref. 32.

Transcriptomics Analysis. In RNAseq, libraries were sequenced on HiSeq 2000 (Illumina, Inc., San Diego, CA, USA). mRNA levels were determined by qRT-PCR. ChIP assays and transcriptional assays were conducted as described elsewhere (19, 34).

Statistical Analysis. Statistical analysis of the data shown in this study was performed using Prism for Mac 8.3 (GraphPad Software, Boston, MA, USA). Bar graphs throughout the manuscript are the mean with SEM. Statistical significance was assessed with a nonparametric Mann–Whitney *U* test. Where appropriate, relevant comparisons were labeled as either significant at the $P \leq 0.001$ (***), $P \leq 0.01$ (**), or $P \leq 0.05$ (*) levels, or nonsignificant for values of $P > 0.05$.

Data, Materials, and Software Availability. RNAseq data have been deposited at National Center for Biotechnology Information Gene Expression Omnibus under accession GSE179619 (37).

ACKNOWLEDGMENTS. We are indebted to researchers who provided us with reagents (*SI Appendix*, *Supplementary Discussion*). Parts of this article related to ZEB1 were developed from C.N.'s PhD dissertation. We express our gratitude to A. Zorzano (University of Barcelona and Institute for Research in Biomedicine of Barcelona, Spain) and A. Cuadrado (University Autonoma of Madrid School of Medicine, Spain) for insightful comments on the manuscript. We are thankful to M Batlle (IDIBAPS) for advice on and sharing of the Amplex® Ultra-Red reagent, Dr. X. Solé (Hospital Clínic de Barcelona, Spain) for advice on the statistical analysis, and B. Martin (CNAG-CRG, Barcelona, Spain) for bioinformatics analysis of RNAseq data. We acknowledge technical assistance by staff in the Transmission Electron Microscopy Unit at the University of Barcelona School of Medicine. IDIBAPS is partly funded by the CERCA Programme of Generalitat de Catalunya. The study was conducted at IDIBAPS' Centre de Recerca Biomèdica Cellex building, which was partly funded by the Cellex Foundation. The different parts of this study were independently funded by grants to A.P. from Duchenne Parent Project Spain (DPPE/01_2018), the Catalan Agency for Management of University and Research Grants (AGAUR) (2021-SGR 01328), and the Spanish State Research Agency (AEI) of the Spanish Ministry of Science and Innovation (PID2020-116338RB-I00) as part of the 2021-2023 Plan for Scientific and Technical Research and Innovation (PEICTI), which is co-financed by the European Regional Development Fund of the European Union Commission. L.H. is supported by a PhD scholarship from the China Scholarship Council (202208110041).

Author affiliations: [a]Group of Gene Regulation in Stem Cells, Cell Plasticity, Differentiation, and Cancer, Institute of Biomedical Research August Pi Sunyer (IDIBAPS), Barcelona 08036, Spain; [b]National Center of Biotechnology (CSIC-CNB) and Center for Molecular Biology Severo Ochoa (CSIC-CBMSO), Transgenesis Facility, High Research Council (CSIC) and Autonomous University of Madrid, Cantoblanco, Madrid 28049, Spain; [c]Group of Muscle Research and Mitochondrial Function, Institute of Biomedical Research August Pi Sunyer (IDIBAPS), University of Barcelona School of Medicine, Hospital Clínic of Barcelona, and Rare Diseases Networking Biomedical Research Center (CIBERer), Barcelona 08036, Spain; [d]National Center for Genomics Analysis (CNAG), Barcelona 08028, Spain; [e]Department of Biomedicine, University of Barcelona School of Medicine, and Institute of Biomedical Research August Pi Sunyer (IDIBAPS), Barcelona 08036, Spain; [f]Molecular Targets Program, Department of Medicine, James Graham Brown Cancer Center, Louisville, KY 40202; and [g]Catalan Institution for Research and Advanced Studies (ICREA), Barcelona 08010, Spain

1. H. Sies, D. P. Jones, Reactive oxygen species (ROS) as pleiotropic physiological signalling agents. *Nat. Rev. Mol. Cell Biol* **21**, 363–383 (2020).
2. H. J. Forman, H. Zhang, Targeting oxidative stress in disease: Promise and limitations of antioxidant therapy. *Nat. Rev. Drug Discov.* **20**, 689–709 (2021).
3. R. Sartori, V. Romanello, M. Sandri, Mechanisms of muscle atrophy and hypertrophy: Implications in health and disease. *Nat. Commun* **12**, 330 (2021).
4. M. C. Gomez-Cabrera *et al.*, Redox modulation of muscle mass and function. *Redox Biol.* **35**, 101531 (2020).
5. C. Mammucari *et al.*, FoxO3 controls autophagy in skeletal muscle in vivo. *Cell Metab.* **6**, 458–471 (2007).
6. K. Min *et al.*, Mitochondrial-targeted antioxidants protect skeletal muscle against immobilization-induced muscle atrophy. *J. Appl. Physiol.* **111**, 1459–1466 (2011).
7. A. Cuadrado *et al.*, Therapeutic targeting of the NRF2 and KEAP1 partnership in chronic diseases. *Nat. Rev. Drug Discov.* **18**, 295–317 (2019).
8. L. Baird, M. Yamamoto, The molecular mechanisms regulating the KEAP1-NRF2 pathway. *Mol. Cell Biol.* **40**, e00099-20 (2020).
9. L. Baird, D. Llères, S. Swift, A. T. Dinkova-Kostova, Regulatory flexibility in the Nrf2-mediated stress response is conferred by conformational cycling of the Keap1-Nrf2 protein complex. *Proc. Natl. Acad. Sci. U.S.A.* **110**, 15259–15264 (2013).
10. A. Cuadrado *et al.*, Transcription factor NRF2 as a therapeutic target for chronic diseases: A systems medicine approach. *Pharmacol. Rev* **70**, 348–383 (2018).
11. M. R. de la Vega, E. Chapman, D. D. Zhang, NRF2 and the hallmarks of cancer. *Cancer Cell* **34**, 21–43 (2018).
12. J. D. Hayes, A. T. Dinkova-Kostova, K. D. Tew, Oxidative stress in cancer. *Cancer Cell* **38**, 167–197 (2020).
13. D. C. Radisky *et al.*, Rac1b and reactive oxygen species mediate MMP-3-induced EMT and genomic instability. *Nature* **436**, 123–127 (2005).
14. A. Postigo, D. C. Dean, Differential expression and function of members of the zfh-1 family of zinc finger/homeodomain repressors. *Proc. Natl. Acad. Sci. U.S.A.* **97**, 6391–6396 (2000).
15. E. Sánchez-Tilló *et al.*, EMT-activating transcription factors in cancer: Beyond EMT and tumor invasiveness. *Cell Mol. Life Sci.* **69**, 3429–3456 (2012).
16. S. Brabletz, H. Schuhwerk, T. Brabletz, M. P. Stemmler, Dynamic EMT: A multi-tool for tumor progression. *EMBO J.* **40**, e108647 (2021).
17. A. Akhmetkaliyev, N. Alibrahim, D. Shafiee, E. Tulchinsky, EMT/MET plasticity in cancer and Go-or-Grow decisions in quiescence: The two sides of the same coin? *Mol. Cancer* **22**, 90 (2023).
18. M. Schuler, F. Ali, E. Metzger, P. Chambon, D. Metzger, Temporally controlled targeted somatic mutagenesis in skeletal muscles of the mouse. *Genesis* **41**, 165–170 (2005).
19. L. Siles, C. Ninfali, M. Cortés, D. S. Darling, A. Postigo, ZEB1 protects skeletal muscle from damage and is required for its regeneration. *Nat. Commun.* **10**, 1364 (2019).
20. D. Roussel *et al.*, Threshold effect in the H2O2 production of skeletal muscle mitochondria during fasting and refeeding. *J. Exp. Biol.* **222**, jeb196188 (2019).
21. A. S. Rambold, E. L. Pearce, Mitochondrial dynamics at the interface of immune cell metabolism and function. *Trends Immunol.* **39**, 6–18 (2018).
22. V. Romanello, M. Sandri, The connection between the dynamic remodeling of the mitochondrial network and the regulation of muscle mass. *Cell Mol. Life Sci.* **78**, 1305–1328 (2021).
23. V. Romanello, M. Sandri, Implications of mitochondrial fusion and fission in skeletal muscle mass and health. *Semin. Cell Dev. Biol.* **143**, 46–53 (2022).
24. V. Romanello *et al.*, Mitochondrial fission and remodelling contributes to muscle atrophy. *EMBO J.* **29**, 1774–1785 (2010).
25. M. Quattrocelli *et al.*, Muscle mitochondrial remodeling by intermittent glucocorticoid drugs requires an intact circadian clock and muscle PGC1α. *Sci. Adv.* **8**, eabm1189 (2021).
26. R. T. Jagoe, S. H. Lecker, M. Gomes, A. L. Goldberg, Patterns of gene expression in atrophying skeletal muscles: Response to food deprivation. *FASEB J.* **16**, 1697–1712 (2002).
27. S. H. Lecker *et al.*, Multiple types of skeletal muscle atrophy involve a common program of changes in gene expression. *FASEB J.* **18**, 39–51 (2004).
28. J. M. Sacheck *et al.*, Rapid disuse and denervation atrophy involve transcriptional changes similar to those of muscle wasting during systemic diseases. *FASEB J.* **21**, 140–155 (2007).
29. G. Milan *et al.*, Regulation of autophagy and the ubiquitin–proteasome system by the FoxO transcriptional network during muscle atrophy. *Nat. Commun.* **6**, 6670 (2015).
30. S. Schiaffino, C. Reggiani, Fiber types in mammalian skeletal muscles. *Physiol. Rev.* **91**, 1447–1531 (2011).
31. D. Sebastián, A. Zorzano, Self-eating for muscle fitness: Autophagy in the control of energy metabolism. *Dev. Cell* **54**, 268–281 (2020).
32. A. E. Frazier, A. E. Vincent, D. M. Turnbull, D. R. Thorburn, R. W. Taylor, "Assessment of mitochondrial respiratory chain enzymes in cells and tissues" in *Mitochondria*, L. A. Pon, E. A. Schon, Eds. (*Methods in Cell Biology*, Elsevier, 2020), vol. 155, pp. 121–156.
33. M. Dodson *et al.*, Modulating NRF2 in disease: Timing is everything. *Ann. Rev. Pharmacol. Toxicol.* **59**, 555–575 (2019).
34. C. Ninfali, L. Siles, D. S. Darling, A. Postigo, Regulation of muscle atrophy-related genes by the opposing transcriptional activities of ZEB1/CtBP and FOXO3. *Nucleic Acids Res* **46**, 10697–10708 (2018).
35. R. Sekido, The δ-crystallin enhancer-binding protein δEF1 is a repressor of E2-box-mediated gene activation. *Mol Cell Biol.* **14**, 5692–5700 (1994).
36. J. E. Remacle, New mode of DNA binding of multi-zinc finger transcription factors: δEF1 family members bind with two hands to two target sites. *EMBO J.* **18**, 5073–5084 (1999).
37. C. Ninfali, A. Esteve-Codina, A. Postigo, Gene expression profile (RNAseq) in atrophic gastrocnemius muscle of wild type, ZEB1 and ZEB2 knock out mice. NCBI's GEO (Gene Expression Omnibus) database. https://www.ncbi.nlm.nih.gov/geo/query/acc.cgi?acc=GSE179619. Deposited 7 July 2021.